Effect of nearest-neighbor ions on excited ionic states, emission spectra, and line profiles in hot and dense plasmas

D. Salzmann
Soreq Nuclear Research Center, Atomic Energy Comission, Yavne, 70600, Israel

J. Stein* and I. B. Goldberg
Racah Institute of Physics, The Hebrew University of Jerusalem, Jerusalem, 91904, Israel

R. H. Pratt
Department of Physics and Astronomy, University of Pittsburgh, Pittsburgh, Pennsylvania 15260
(Received 26 November 1990)

A two-center model is used to study the influence of the cylindrical symmetry, imposed by the nearest neighbor, on the ionic levels and emission spectra of a Li-like krypton ion immersed in hot and dense plasma. The symmetry breaking of the spherical symmetry of the local microfield in the peripheries of the ion due to the effect of its nearest neighbor is accounted for by expanding the total electric microfield into its multipole components. The resulting cylindrically symmetric Hamiltonian is diagonalized to obtain the energy levels in this distorted microfield. It is shown that the cylindrical symmetry mixes states with different l's (l is the orbital quantum number), particularly for highly excited states, and thereby gives rise to forbidden transitions in the emission spectrum. Results are obtained for (i) the variation of the ionic level shifts and mixing coefficients with the distance to the nearest neighbor and (ii) representative computed spectra to show the density effects on the spectral line profiles, shifts, and widths, and the forbidden components in the spectrum. It is found that by an ion density of 3×10^{22} cm^{-3} forbidden lines can be of the same magnitude as the original allowed lines. Linewidths resulting from the distribution of nearest-neighbor distances are narrower than the result from the mechanism of Woltz and Hooper [Phys. Rev. A **38**, 4766 (1988)]. Mixing is not important for the dominant ground-state configuration species of the plasma but rather enters through its major effects on excited-state properties.

I. INTRODUCTION

The density and temperature dependence of the atomic energy levels and the spectra of ions immersed in hot and dense plasmas have been investigated for many years by means of various models. The earlier models incorporated the effects of the plasma environment on the atomic properties of the plasma ions by using a density- and temperature-dependent quantity $\Delta E(n_i,T)$, called the ionization energy lowering [1]. Later, the ion-sphere model [2–4] and the density-functional theory [5], in their various versions, became popular, introducing more detailed modeling of plasma environment effects on the atomic potential in the neighborhood of plasma ions. The common feature to all these models is the assumption of a spherically symmetric environment around the ion.

The spherically symmetric models are expected to give a rather good physical picture well within the ion-sphere radius, i.e., for inner ionic levels and high-energy continuum states. However, for a better understanding of atomic properties of ions with electrons in excited bound states, or low-energy continuum states, whose wave functions are large in the outer volume of the ions and the interionic space, a more realistic description of the symmetry of the local microfield around the ion is necessary. In these outer regions, where the influence of neighboring ions is greater, the electric field cannot be regarded as spherically symmetric anymore.

Recently, several attempts have been made to incorporate the alteration of the local electric microfield around a given ion from a spherical symmetry at low densities, to cylindrical symmetry at intermediate densities, and to cubic symmetry at very high densities. Younger *et al.* [6] carried out a full systematic quantum-mechanical calculation of a high-energy-density plasma which included nine helium atoms positioned in a body-centered-cubic cluster. From their studies they identified four regions of atomic behavior, depending on the ratio between the bound electron wavelength and the interionic distance. Recently, they extended their studies [7] to calculate many-electron effects on the dynamical correlations in dense helium plasma by formulating a self-consistent-field molecular dynamics. In their recent simulations they used up to 30 helium atoms, thereby greatly improving the validity of their model. Their method gives an insight into the atomic properties of ions at intermediate densities (0.1 and 1.5 g/cm^3, 1.5×10^{22} and 2.25×10^{23} atoms/cm^3) and temperatures (1 and 5 eV) which so far cannot be attained by other models. At these rather low temperatures the atomic excitation and ionization processes were omitted. The application of their method to other atoms and temperatures is, however, not straightforward.

In our previous work (Ref. [8], heretoforth referred to as I) we used the observation that when the plasma coupling parameter Γ is not very large, the probability of finding one of the neighboring ions significantly closer than the others is quite large. The screening of the ionic interaction by the free electrons makes the ion-ion interaction potential a highly nonlinear function of the interionic distance, which diminishes rapidly at larger distances. Therefore, as a first correction to the ion-sphere model we considered the ion and its nearest neighbor as a quasimolecule and accounted for the further plasma effects by assuming a finite volume of a particular shape for this quasimolecule. This is a generalization of the ion-sphere model. In our model the local microfield deviated substantially from the spherical symmetry, due to the nearest neighbor which imposes a cylindrical symmetry on the peripheries of the ion. This symmetry breaking is analyzed through its multipole components. In I we gave results for the thermodynamic properties (free energy, average interionic distance, ionization potential lowering) for an iron plasma at densities around 10^{23} cm^{-3} and temperatures from 30 up to 3000 eV.

Following a similar idea, Malnoult, d'Etat, and Nguyen [9] in a recent paper solved the Schrödinger equation for a two-ion-center problem by using elliptic coordinates. They assumed an electrically neutral system of two ions and a homogeneous electron distribution in a cylindrically symmetric volume. The shape of the boundary of their volume is a Coulomb equipotential surface of two point charges separated by the interionic distance R. Such a boundary results in electric fields outside the quasimolecular volume. In comparison with our work the description of the potential and its volume has been simplified, while a full molecular rather than an atomic calculation has been performed. They presented results for the equipotentials of hydrogenlike ions, and for the frequency shift of Ne X Lyman-α line as a function of the distance to the nearest neighbor. They found drastic reductions in Stark shifts and possibly new spectral components.

In the present paper we extend our model (I) to include computations of the line profiles, shifts, and widths, as well as the energy-level mixing and the forbidden transition probabilities. Spectra from excited states of Li-like krypton ions in dense and hot plasmas are used to illustrate our studies. We particularly focus on the influence of the increasing plasma density on the energy-level shifts, level mixing, emission spectrum, forbidden transitions, line profiles, and shifts. In our model we continued to use symmetric quasimolecules, while in the real plasma the nearest neighbor may have a different electronic configuration than the perturbed ion. This could not have a large effect on the nature of the perturbation when the ions are highly ionized and the fluctuation of the number of bound electrons is small relative to the average ionization.

Our choice of krypton plasma was influenced by a recent paper of Woltz and Hooper [10], who simulated experimental spectra obtained at the Laboratory for Laser Energetics, University of Rochester. Their formalism includes a quantum-mechanical relaxation theory [11] for the plasma electron broadening (found not important), and a static ion approximation for the plasma ion broadening. They found that assuming a homogeneous plasma with a temperature of 1100 eV and an electron density of 2×10^{23} cm^{-3} their computed spectra for a combined Be-like and Li-like krypton plasma reproduced the experimental results with reasonable accuracy. (For simplicity we have confined our attention to the Li-like case.)

In Sec. II the basics of our model (I) are briefly reviewed, developing features and introducing changes needed for the discussion of spectra, and with emphasis on some subsequent improvements in the model. In Sec. III we give details of the calculation of the spectrum and present computed spectra for Li-like krypton. Atomic units ($e^2=m=\hbar=1$) are used throughout.

II. CYLINDRICALLY SYMMETRIC ATOMIC MODEL

A. The basic assumptions of the model

Our starting point is the notion that when two neighboring ions approach each other the symmetry of the potential within the region of either ion changes from a spherical to a cylindrical one, with the symmetry axis along the line connecting the two ions. While the innermost bound electrons are perturbed only slightly by this symmetry change, the highly excited states could be deformed so strongly that they overlap both ions, thereby generating real short-lived quasimolecular states. Such states will not be considered here.

In our model the shape of this molecular volume is approximated by two adjacent truncated spheres (see Fig. 1), each having volume τ. Our model concerns an atomic calculation within one of these truncated spheres. It was shown in Ref. [12] that for constant electron density the electric field in such a quasimolecular volume vanishes on the boundaries, if these boundaries have a particular peanutlike shape. For such a peanut-shaped molecular volume the potential energy is minimum for variations of the boundaries which keep the volume constant. This result was generalized in I to a Thomas-Fermi (TF) distribution of electrons, where it was found that a similar

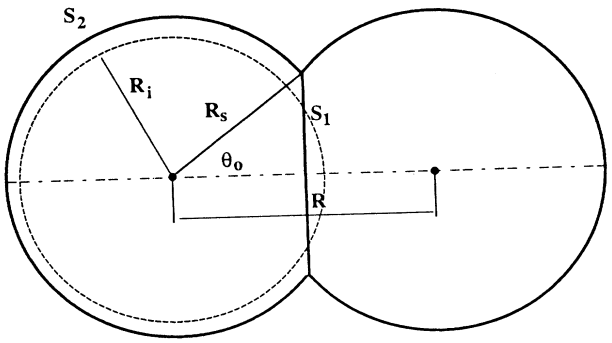

FIG. 1. Approximate shape of the quasimolecule.

peanut shape, for which the electric field vanishes on the boundary of the quasimolecule, minimizes the free energy of the electrons in the TF model too (rather than the potential energy). In a plasma of high temperature, with an almost homogeneous electron density over most of the ionic volume, the TF shape should be almost identical to the corresponding peanut shape of Ref. [12]. In paper I it was shown that while replacing the ideal peanut shape with the truncated sphere shape introduces inaccuracies of the order of a few percent into the model, it allows the setup of the mathematical equations with convenient boundary conditions.

The volume of each truncated sphere is kept equal to the ion-sphere volume,

$$\tau=\frac{1}{n_i}=\frac{4\pi}{3}R_i^3 \tag{2.1}$$

(n_i is the ion number density and R_i is the ion-sphere radius). This puts a constraint on the radius of the outer surface R_s, which is computed from the equation

$$\tau=\pi(\tfrac{2}{3}R_s^3+\tfrac{1}{2}R_s^2R-\tfrac{1}{24}R^3) . \tag{2.2}$$

Here R is the distance between the two ions (see Fig. 1). The reason for keeping τ constant, unlike in the TF case of I, is that here we are keeping a fixed configuration of bound electrons, i.e., a fixed number of free electrons. Keeping the Fermi energy constant here would have changed the density by 2.3% between $R=2R_i$ and $0.7R_i$. The effect on the line shape would be very small.

The Born-Oppenheimer approximation has been used here, as it had been used in Ref. [10] (to which we compare our results), even though the average ion-ion collision time t is such that $2\pi\hbar/t$ is of the same order of magnitude as the differences between some pairs of $n=4$ levels.

To account for the cylindrical symmetry, the potential is expanded into its multipole components,

$$V(\mathbf{r};R)=V_0(r)+\sum_{k=0}^{\infty}v_k(r;R)P_k(\cos\theta) , \tag{2.3}$$

which depend on the distance to the nearest neighbor as well. In (2.3) $V_0(r)$ is the spherically symmetric potential, discussed in detail below. $P_k(\cos\theta)$ are the Legendre polynomials and $v_k(r;R)$ are the multipole components to be determined. The correction to V_0 was obtained perturbatively (first-order correction only); the multipole expansion of the first-order correction converged reasonably well.

The total potential $V(\mathbf{r};R)$ has to satisfy three boundary conditions.

(i) Near the nucleus the potential is Coulombic,

$$\lim_{r\to 0} rV(\mathbf{r};R)=Ze , \tag{2.4}$$

where Z is the nuclear charge.

(ii) On the surface S_1 the normal electric field, i.e., the normal derivative of the potential, should vanish:

$$\left.\frac{\partial V(\mathbf{r};R)}{\partial n}\right|_{S_1}=\left.\frac{\partial V(\mathbf{r};R)}{\partial z}\right|_{z=R/2}=0 , \tag{2.5}$$

where z is the coordinate along the symmetry axis.

(iii) One would also like the total electric field to vanish on the spherical surface S_2 of the truncated sphere. This condition would mean that there is no electric field outside the volume, so that the quasimolecular volume is electrically isolated and the electronic free energy is at a minimum with respect to shape variations. This condition, however, cannot be satisfied rigorously, because the shape of the volume is already determined. Instead, two weaker conditions are imposed: (a) the molecular volume is electrically neutral, and (b) the potential vanishes on the outer boundary S_2, i.e.,

$$\int_{S_2}\frac{\partial V}{\partial n}dS=0 , \tag{2.6a}$$

$$V(R_s;R)=0 . \tag{2.6b}$$

Equation (2.3) with the boundary conditions (2.4), (2.5), (2.6a), and (2.6b) has a unique solution.

In I a rather thorough investigation was carried out as to how accurately E vanishes on the boundaries with these assumptions. For a range of densities and temperatures it was found that the electric field on the boundaries S_1 and S_2 is small, thereby confirming the basic claim that the approximate shape of the quasimolecular volume is sufficiently close.

Between the model as presented in I and the present paper there is one significant difference. In I we used the Thomas-Fermi model to calculate the electric potential around the ion. In the Thomas-Fermi model the fraction of bound and free electrons is determined within the model and changes with the interionic distance; the fraction has meaning only in an average sense. Such an approach is more appropriate for the calculation of thermodynamic quantities. In the present paper our interest is the profile of a particular spectral line corresponding to a transition between two given electronic configurations. Therefore, we cannot use the Thomas-Fermi model for the bound electrons. Instead, we used a Hartree-Dirac method for the bound electrons and a Thomas-Fermi method for the free electrons, with the free-electron density as given below in Sec. II C.

B. Calculation of the nearest-neighbor perturbation

Substitution of our trial potential, Eq. (2.3), into the Poisson equation

$$\nabla^2V(\mathbf{r};R)=-4\pi[\bar{Z}n_i(r)-n_b(r)-n_f(r)] \tag{2.7}$$

[$n_f(r)$ and $n_b(r)$ are the free- and bound-electron densities, respectively, and $\bar{Z}$ is the average charge of the ion] yields a nonlinear partial differential equation for the potential V. As in I we use first-order linearization of (2.7) to produce a second order linear inhomogeneous differential equation for the multipole components,

$$v_k''+\frac{2}{r}v_k'-\frac{k(k+1)}{r^2}v_k=\frac{2\pi e^2}{kT}\frac{1}{2\pi^2}\left[\frac{2mkT}{\hbar^2}\right]^{3/2}\left[F_{-1/2}(x_0+\beta_0,\beta_0)(v_k+\eta\delta_{k,0})+\frac{\beta_0^{1/2}\eta\delta_{k,0}}{\exp(-x_0)+1}\right],$$

$$x_0=\frac{\varepsilon_F^0}{kT},\quad \beta_0=\frac{eV_0}{kT}. \tag{2.8}$$

Here $F_j(x;\beta)$ is the incomplete Fermi-Dirac function of the order j defined by

$$Fj(x;\beta)=\int_\beta^\infty \frac{y^j}{\exp(y-x)+1}dy , \tag{2.9}$$

and ε_F^0 is the chemical potential, which is determined from the constraint,

$$Z_f=\int_\tau n_f(r;\varepsilon_F)d^3r , \tag{2.10}$$

where Z_f is the number of free electrons per ion. Equations (2.8) is to be solved for the multipole components of the total potential. In (2.8)

$$\eta=(\varepsilon_F-\varepsilon_F^0)/e \tag{2.11}$$

is the difference between the spherically symmetric and cylindrically symmetric values of the chemical potential. As mentioned above, ε_F and η are functions of the interionic distance R.

The boundary condition Eq. (2.4) implies

$$\lim_{r\to 0} rv_k(r)=0 . \tag{2.12}$$

The other boundary conditions Eqs. (2.5) and (2.6) couple the various v_k's and thus determine the particular solution of Eq. (2.8).

In practice, only a finite number of terms (generally $k\leq 30$) were taken into account in the expansion of Eq. (2.3), and therefore the boundary conditions can be satisfied only approximately. The details of our approximation, using a least-squares procedure to minimize the error, would be too lengthy to be repeated here; the interested reader is referred to I.

C. The choice of the spherically symmetric zeroth-order potential $V_0(r)$

In the present paper we focused on ions with well-defined electronic configuration. More specifically, we illustrate the results of our cylindrically symmetric quasimolecular model by calculating the various features of the emission spectrum of lithiumlike krypton at various densities. For such a constant configuration the statistical potential of the Thomas-Fermi model, which is based on statistical occupation numbers, is inappropriate. To better simulate the potential of constant configurations, the zeroth-order spherically symmetric potential $V_0(r)$ is computed from a relativistic Hartree-Dirac type code [13] which solves the Dirac equation in an ion sphere of radius R_i by treating self-consistently the bound and free electrons. Details of the method are given in Ref. [13]. Note that the radius of this sphere is the ion-sphere radius R_i, and is smaller than the radius R_s of the truncated sphere in which we calculate our first-order corrections to the potential. $V_0(r)$ vanishes outside the ion sphere. In this code, based on the ion-sphere model, the bound-electron wave functions are calculated directly by solving the relativistic Dirac equation. The free electrons are treated statistically by using the incomplete Fermi-Dirac functions to compute their spatial distribution. More accurately, the potential generated by the electrons is obtained from the Poisson equation,

$$\nabla^2V_e(r)=4\pi[n_f(r)+n_b(r)] . \tag{2.13}$$

The total potential is

$$V_0(r)=-Z/r+V_e(r) . \tag{2.14}$$

The bound-electron eigenvalues and wave functions are obtained by solving the relativistic Dirac equation

$$[i\hbar c\boldsymbol{\alpha}\cdot\nabla-\beta mc^2+eV_0(r)]\psi_{n\kappa m}^0=\varepsilon_{n\kappa m}^0\psi_{n\kappa m}^0 \tag{2.15}$$

in this central potential. In (2.15) α and β are the Dirac matrices, $\varepsilon_{n\kappa m}^0$ is the total (including the rest mass) energy of the bound electron, and $\psi_{n\kappa m}^0$ is the eigenfunction with the corresponding quantum numbers $\kappa=(-1)^{j+l+1/2}(j+\frac{1}{2})$ and m. From these wave functions the bound-electron density can be calculated as

$$n_b(r)=\sum_{n,\kappa}(2j+1)|\psi_{n\kappa}^0|^2 . \tag{2.16}$$

The free-electron spatial distribution within the ion sphere is assumed to follow Fermi-Dirac statistics:

$$n_f(r)=\frac{2}{(2\pi\hbar)^3}\times\int_{p^2/2m>V_0}\frac{d^3p}{\exp[(p^2/2m-V_0-\varepsilon_F^0)/kT]+1}$$

$$=\frac{1}{2\pi^2}\left[\frac{2mkT}{\hbar^2}\right]^{3/2}F_{1/2}\left[\frac{\varepsilon_F^0+V_0(r)}{kT};\left|\frac{eV_0(r)}{kT}\right|\right] . \tag{2.17}$$

Equations (2.13)–(2.17) are solved self-consistently for the bound and free electrons.

The code has the option to include various versions of exchange interactions. These were not used in the calculation of $V_0(r)$, because the Slater-type long-range exchange potentials extend beyond the truncated sphere boundaries, and their validity near the boundaries is questionable. However, this approximation was used only for calculating the perturbation to the potential due to the interaction with the nearest neighbor. We did in-

clude the exchange interaction in the calculation of the bound-state energy levels ε^0_{njlm} and wave functions ψ^0_{njlm}. The Latter tail was not incorporated in the asymptotic behavior of the potential.

D. Zeroth-order dipole matrix elements

Having the above atomic quantities, a second code was used to calculate the zeroth-order dipole transition matrix elements between any two bound levels $\langle a|H'|b\rangle$ and the corresponding oscillator strengths for this spherically symmetric potential. For these computations we used the relativistic formulas for single-electron transitions given by Grant [14]. Since initial and final states correspond to different configurations, they are being calculated in different potentials; the small cross terms arising from this lack of orthogonality have been neglected.

E. Probability density function for the distance to the nearest neighbor

Finally, the total cylindrically symmetric potential $V(\mathbf{r};\mathbf{R})$ in Eq. (2.3) was used to compute the electron-electron, ion-ion, and electron-ion interaction terms as well as the total kinetic energy in order to get the free energy of the two-body system (see I)

$$F(R)=E+PV-TS\ , \tag{2.18}$$

$$E=E_p^{e\text{-}e}+E_p^{e\text{-}i}+E_p^{i\text{-}i}+E_k^e\ . \tag{2.19}$$

As shown in I, $F(R)$ is a monotonically, rather steeply, decreasing function of the distance to the nearest neighbor.

By using this free energy as an effective ion-ion potential one can, in principle, calculate the probability density $P(x)$ for having the nearest neighbor at a distance between $x=R/R_i$ and $x+dx=(R+dR)/R_i$. Given a distribution of N ions in a volume V, the probability of having the ions at the infinitesimal volumes $d^3r_1, d^3r_2, \ldots, d^3r_N$, positioned around the points $\mathbf{r}_1, \mathbf{r}_2, \ldots, \mathbf{r}_N$ is proportional to the weight function

$$W(\mathbf{r}_1,\mathbf{r}_2,\ldots,\mathbf{r}_N)d^3r_1,d^3r_2,\ldots,d^3r_N = \exp\left[-\frac{1}{kT}\sum_{i,j}F(|\mathbf{r}_i-\mathbf{r}_j|)\right]d^3r_1,d^3r_2,\ldots,d^3r_N\ . \tag{2.20}$$

Using this weight function we have applied a Monte Carlo method to compute the first three moments of $P(x)$. The probability function was approximated by

$$P(x)=Ax^2\exp(-x^3-B/x+Cx+Dx^2)\ . \tag{2.21}$$

A is a normalization constant and B, C, and D are determined from these three moments. (In an uncorrelated plasma $B=C=D=0$.) For small values of x, B/x represents the effect of ion-ion repulsion on the probability. The last two terms in the exponential function are corrections for intermediate values of x. This was sufficiently accurate for calculating the line shapes with our model.

Examples of such results are given in Fig. 2, which shows that there is a probability of more than 0.95 of finding the nearest neighbor in the range $(0.6R_i, 1.7R_i)$ with the most probable distance between $1.1R_i$ and $1.2R_i$. These features are common to the three densities calculated here in the krypton plasma, as well as to iron plasmas at densities of 10^{23} cm^{-3} for temperatures between 15 and 1500 eV, as shown in I. It can be seen that the most probable distance has been pushed out from about $0.9R_i$ of the uncorrelated plasma case, showing the

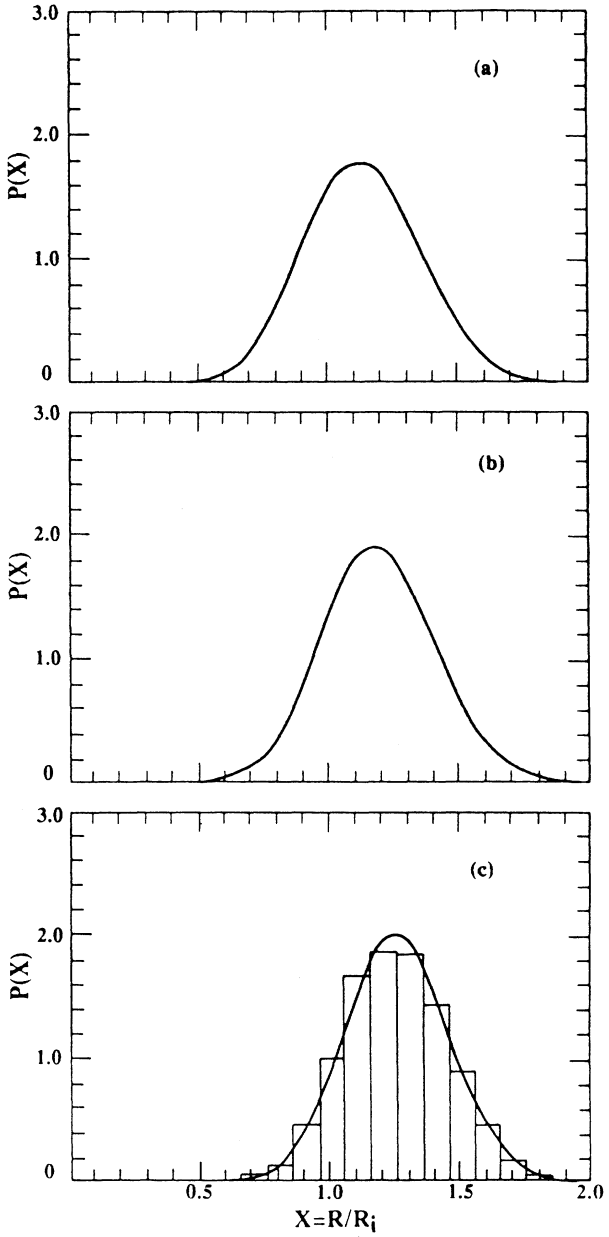

FIG. 2. Probability densities for having the nearest neighbor at distance R in a Li-like krypton plasma at a temperature of 1100 eV and densities of (a) 6×10^{21} cm^{-3}, (b) 3×10^{22} cm^{-3}, (c) 1×10^{23} cm^{-3}. The histogram represents Monte Carlo results from which the probability density moments were derived.

resistance of penetration of ion cores and the corresponding plasma correlation effects.

From the results of the Monte Carlo calculation we could evaluate the average distance to the second nearest neighbor as well. At a density of 3×10^{22} cm^{-3} the average distance to this second neighbor was approximately $1.4R_i$. A rough estimate indicates that this has only minor influence on the ionic levels and wave functions relative to the effects of the first nearest neighbor.

III. CALCULATION OF LINE PROFILES AND FORBIDDEN TRANSITION SPECTRA

Equipped with the above results one has all the tools required to compute the ionic level shifts with respect to the ion-sphere case due to the multipole components of the field, as well as the mixing coefficients among the uppermost bound states. The shifts reduce somewhat the large red shifts of the ion sphere from the free ion. The mixing coefficients $|a_{\mu\nu}(R)|^2$, are defined by means of the expansion coefficients expressing the cylindrically symmetric wave functions in terms of the spherically symmetric ones,

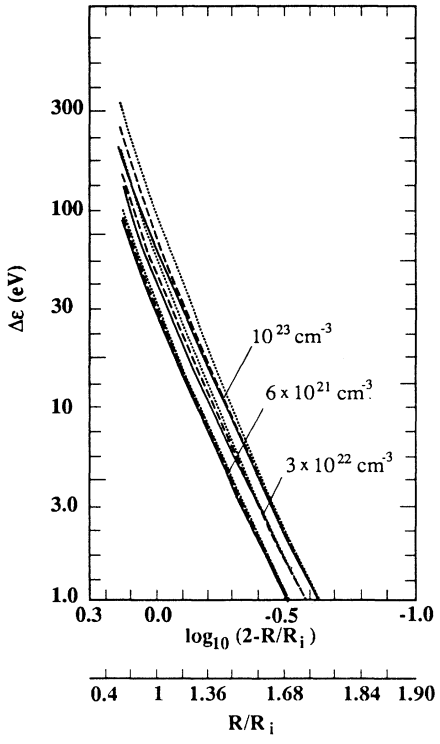

FIG. 3. The difference between the energy levels as calculated in the cylindrically symmetric and the spherically symmetric models, for $T=1100$ eV, (a) $n_i=6\times10^{21}$ cm^{-3}, (b) $n_i=3\times10^{22}$ cm^{-3}, (c) $n_i=1\times10^{23}$ cm^{-3}. For each density the shifts of the $1s$ (uppermost line), $3s$ (dashed line), and $4s$ (lowest line) levels are shown. The line for the $2s$ level is indistinguishable from that of $1s$.

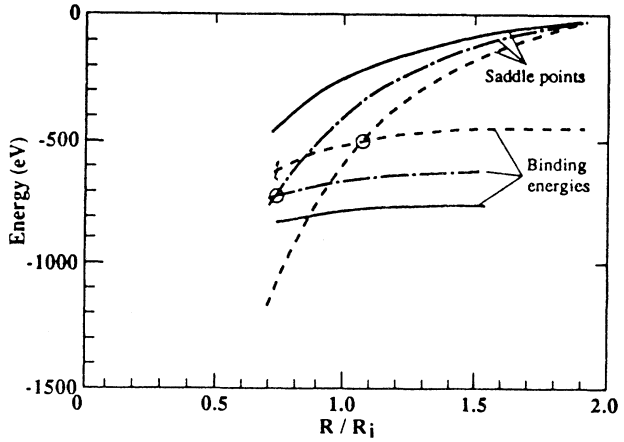

FIG. 4. The energy of the saddle point and the energy of the $4d_{5/2}$ level as a function of R/R_i at three densities: (a) $n_i=6\times10^{21}$ cm^{-3} (solid line), (b) $n_i=3\times10^{22}$ cm^{-3} (dash-dotted line), (c) $n_i=1\times10^{23}$ cm^{-3} (dashed line).

$$\psi_\mu(\mathbf{r};R)=\sum_\nu a_{\mu\nu}(R)\psi_\nu^0(\mathbf{r})\ . \tag{3.1}$$

Interesting features of the multipole distortions show up particularly when the excited bound state is strongly perturbed by the field of the nearest neighbor. In this case the change is too big to be dealt with in terms of a first-order perturbation theory. The Hamiltonian $H_0+\sum_{k=0}^{k^{\max}}v_k(r;R)P_k(\cos\theta)$ was diagonalized by allowing a mixture of states with the same n's and M's (principal and magnetic quantum numbers) but with different l's (orbital quantum number). In fact, only the uppermost states have to be diagonalized, as the inner states are still influenced mainly by the nuclear potential and the mono-

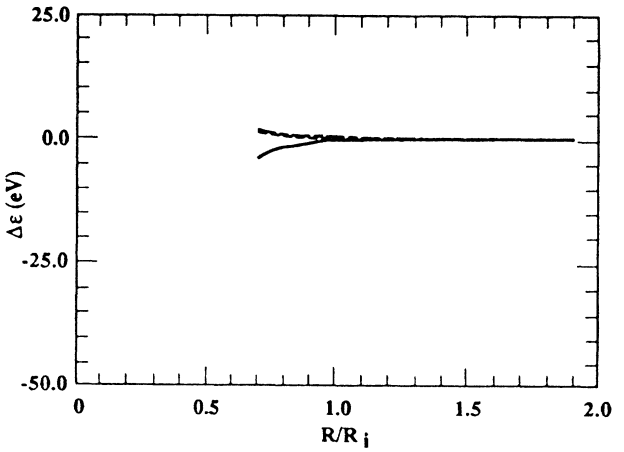

FIG. 5. The splitting of the $n=2$, $M=\frac{1}{2}$ levels due to the multipole components at $n_i=1\times10^{23}$ cm^{-3} as a function of the relative interionic distance R/R_i. For the notation of the sublevels see Fig. 6.

pole component of the perturbation, which are spherically symmetric, and therefore, the original quantum numbers of the inner states $njlm$ are still good quantum numbers. For the upper states, however, the nondiagonal matrix elements in the l submatrices are of the same order of magnitude as the diagonal ones, indicating a strong mixture among the various l's. We considered a space of atomic states up to $n=4$, $l=3$, diagonalizing only within $n=4$.

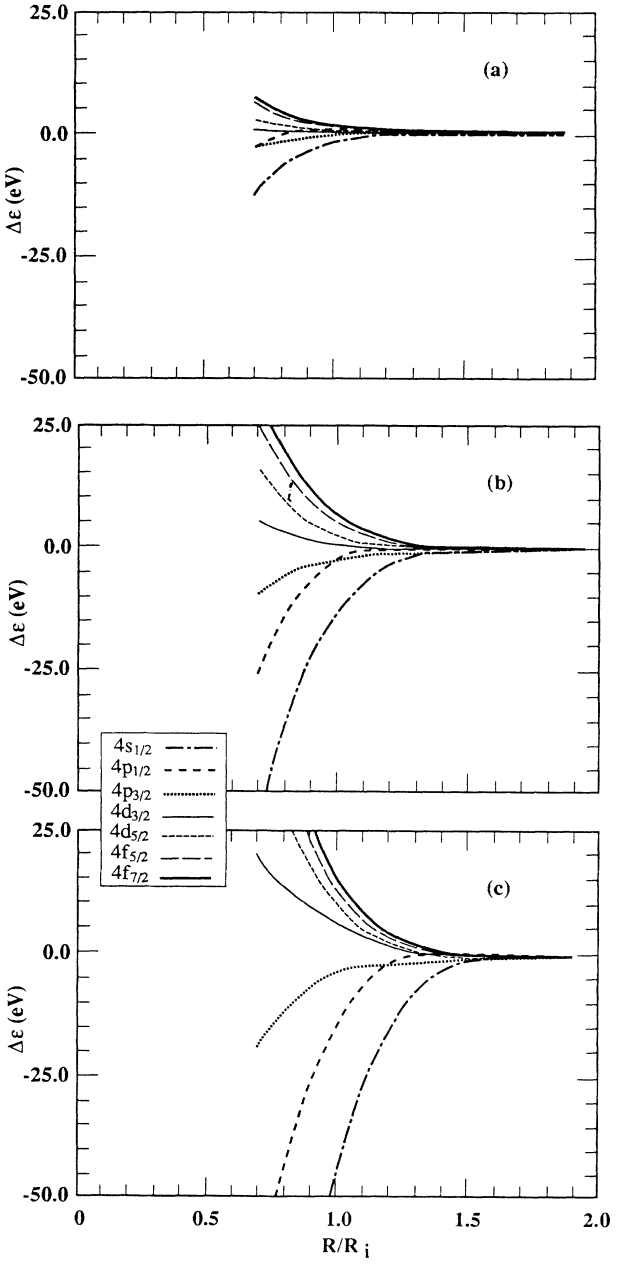

FIG. 6. The same as Fig. 5 for the $n=4$, $M=\frac{1}{2}$ levels. (a) $n_i=6\times10^{21}$ cm^{-3}, (b) $n_i=3\times10^{22}$ cm^{-3}, (c) $n_i=1\times10^{23}$ cm^{-3}. The insert shows the notation of the various sublevels.

A. Level shifts

The difference between the energy levels as calculated by the cylindrically symmetric model and the spherically symmetric solution is shown in Fig. 3 on a log-log scale for a Li-like krypton ion immersed in a plasma of similar ions, at $T=1100$ eV and $n_i=1\times10^{23}$ cm^{-3}. The cylindrically symmetric states are the lower, more bound, ones.

The main cause for the level shifts

$$\Delta\varepsilon_n(R)=\varepsilon_n(R)-\varepsilon_n(2R_i) \tag{3.2}$$

relative to the ion-sphere case is the monopole component of the perturbing field. For the density range presented here, this shift is almost independent of the atomic state, as can be seen from Fig. 3. The average level shift can be approximated by

$$\overline{\Delta\varepsilon_n}(R)=K(n_i)(2-R/R_i)^C \text{ eV} \tag{3.3}$$

for all the atomic states. The constant C is almost independent on the density, being very close to 3. The coefficients $K\simeq30$, 63, and 100 eV for $n_i=6\times10^{21}$, 3×10^{22}, and 1×10^{23} cm^{-3}, respectively, scaling approximately as $K(n_i)=4.5\times10^{-9}\,n_i^{0.45}$ eV.

Figure 4 shows a comparison, at three densities, between the energy at the saddle point, halfway between the two ions, and the average energy of the $4d_{5/2}$ levels. Perturbation expansion is valid only as long as the energy of the bound state is well below the saddle-point energy. Figure 4 shows that this condition holds true for densities of $n_i=6\times10^{21}$ and 3×10^{22} cm^{-3}. However, for $n_i=1\times10^{23}$ cm^{-3} this condition is satisfied only for some R/R_i, therefore results for a line shape which reflect the contributions of the various R's are only of qualitative value for this density.

B. Level splitting and mixing

Figures 5 and 6 show the splitting due to the multipole components $v_k(r;R)$ of the various substates for a given n and M as a function of R/R_i. To emphasize this splitting, we present the energy shift of a given level relative to the energy shift of the ground state,

$$\delta\varepsilon_n(R)=\varepsilon_n(R)-\varepsilon_n(2R_i)-[\varepsilon_{1s}(R)-\varepsilon_{1s}(2R_i)]\ . \tag{3.4}$$

The notation for the states in Figs. 5 and 6 indicates the orbital quantum number that the state would acquire asymptotically in a spherically symmetric field.

In Fig. 5 the splitting of the $n=2$, $M=\frac{1}{2}$ case is shown

as a function of the interionic distance for $n_i = 1 \times 10^{23}$ cm^{-3}. As the $n=2$ states are affected mainly by the spherically symmetric nuclear field, the splitting is rather small even at the average interionic distance $R/R_i \simeq 1.12$ and is appreciable only for low probability close encounters between the ions. For the lower densities the splitting is much smaller.

In Fig. 6 a similar splitting is shown for the $n=4$, $M=\frac{1}{2}$ state. A much larger influence of the nearest-neighbor field on the outer $n=4$ states can be seen. The splitting in this case is significantly greater than in the $n=2$ case, and amounts to 1, 10, and 32 eV at the average interionic distance for the three densities under study.

The mixing coefficients

$$|a(n=4,l,j,M=\tfrac{1}{2};n=4,l',j',M=\tfrac{1}{2})|^2$$

among the $n=4$, $M=\frac{1}{2}$ states in the various subshells are shown in Fig. 7. Generally, the mixing of the lower n states, which are subject to the spherically symmetric nuclear field, is small relative to the mixing among the various $n=4$ states. The figure confirms our expectations that when the nearest neighbor is quite far, the states are pure-l atomic states. It can be seen from Fig. 7 that as the ions come slightly closer, to a distance where still only the dipole component of the potential is effective, mainly some of the $\Delta l = \pm 1$, $\Delta j = 0, \pm 1$ states are mixed into the original state. However, when the ions are closer, so that the quadrupole and higher components are strengthened, also the $\Delta l = \pm 2$ state contribution becomes appreciable. Finally, for close encounters, $R \leq 0.7 R_i$, many states combine almost equally to the cylindrically symmetric wave function. The effect of the density on the mixing can also be seen in Fig. 7. As the density increases the mixing becomes stronger for the same value of R/R_i since the distance of a given state, if it still exists, does not decrease when the density increases.

C. Emission spectrum and forbidden transitions

One very important consequence of the mixing at high densities of the wave functions with various l's is the appearance of forbidden transitions which in a spherically symmetric model would be prohibited due to the orbital quantum number selection rules. In a cylindrically symmetric model such transitions occur through components which are mixed into the original state by the multipole field. The above discussion indicates that the intensity of these forbidden transitions is expected to grow rapidly with decreasing interionic distance and with the increasing ion density in the plasma.

As explained above, the interionic distance R determines uniquely the energy shift for every ionic level $\Delta\varepsilon_n(R)$. The emission line shift, as calculated from the energy difference of any two levels,

$$\Delta h\nu_{nm}(R) = \Delta h\nu^0_{nm} + \Delta\varepsilon_n(R) - \Delta\varepsilon_m(R) \tag{3.5}$$

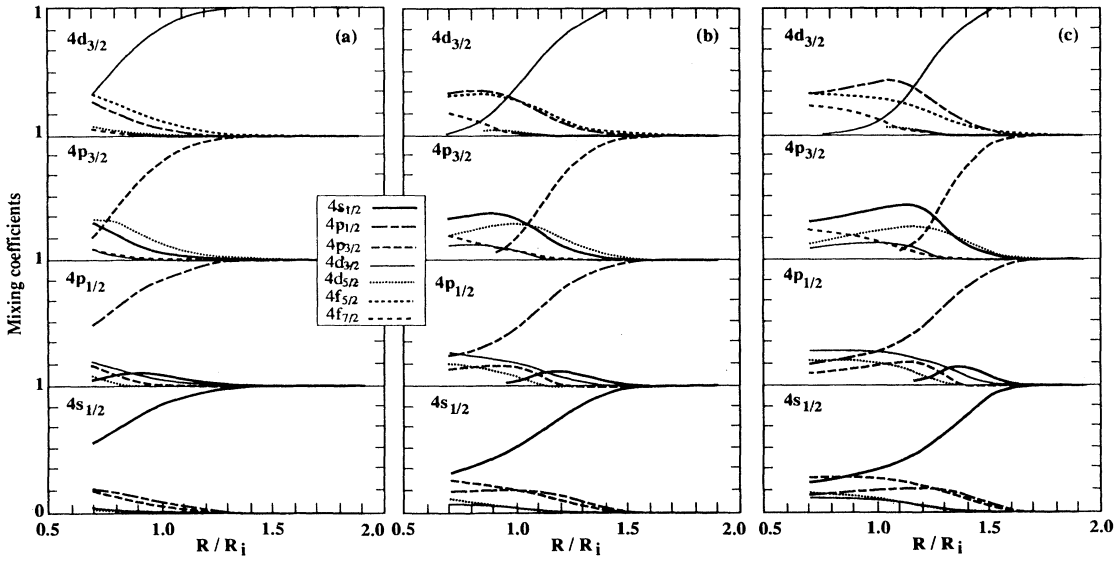

FIG. 7. The mixing coefficients among various sublevels of the $n=4$ state, as a function of the relative interionic distance R/R_i. The inset shows the notation of the various sublevels. Densities are the same as in Fig. 6.

($\Delta h\nu^0_{nm}$ is the line shift as calculated in the spherically symmetric model). Equation (3.5) together with the probability function, $P(R/R_i)$, Eq. (2.21), yield the line profile.

Results of spectra computed from the above model for Li-like Krypton at temperature of 1100 eV and ion densities of 6×10^{21}, 3×10^{22}, and 1×10^{23} cm^{-3} are presented in Figs. 8–10. These spectra were computed also by Woltz and Hooper [10]. The spectra in Figs. 8–10 do not include the negligible broadening due to electron impact [10]. They should be regarded as accounting for the nearest-neighbor quasistatic line broadening and shift. Following Ref. 9, we have also added a 1.5-eV instrumental broadening.

Figures 8–10 show a red shift of the emission spectrum with increasing density. This shift is due to our choice of the zeroth-order potential V_0, in which pure electrostatic interaction is assumed between the bound electrons and the TF free electrons. The adequacy of such potential to describe the interaction of the bound electrons with the

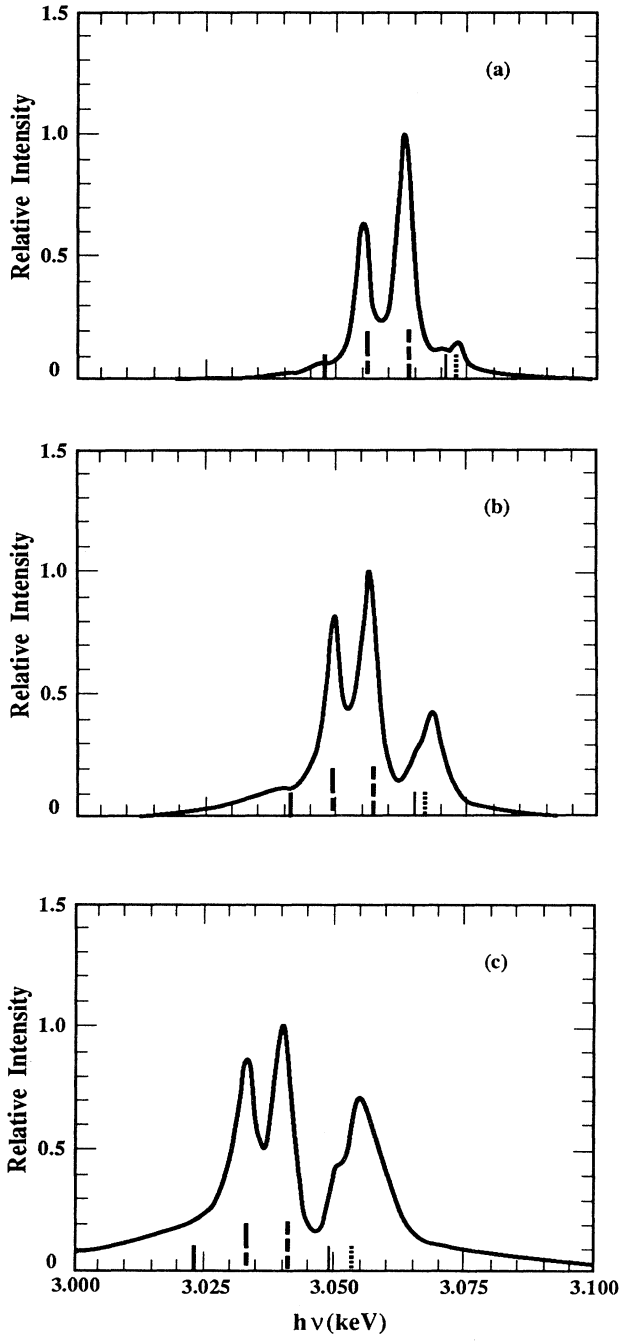

FIG. 8. The computed spectra from the $n=4\rightarrow 2s_{1/2}$ transition. (a) $n_i=6\times10^{21}$ cm^{-3}, (b) $n_i=3\times10^{22}$ cm^{-3}, (c) $n_i=1\times10^{23}$ cm^{-3}. The small vertical lines on the abscissa show the positions of the lines in a spherically symmetric potential. The notation for these lines is the same as in Fig. 7.

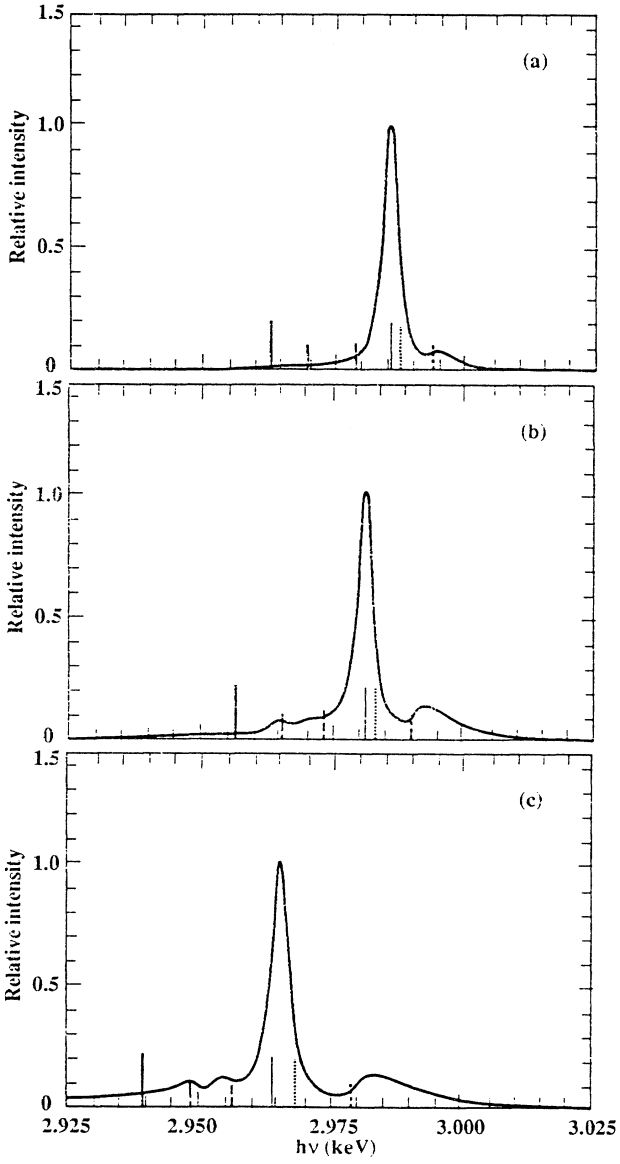

FIG. 9. The same as Fig. 8 for the $n=4\rightarrow 2p_{1/2}$ transition.

free electrons, which penetrate their orbits, has been challenged in the last decade [15–18] but no satisfactory solution has been found yet. However, this shift is very small compared to both the line energies, and teh binding energies, it stems from a very small difference in the potential, mainly in the inner part of the ion sphere, and should cause only a slight difference in the nearest-neighbor interaction potential [Eq. (2.8)]. Consequently the shapes of the lines in Figs. 8–10 are not affected by this shift. The interaction with the deeply penetrating free electrons might, however, affect the line broadening, but this effect is ignored here, and is hopefully covered by the instrumental broadening.

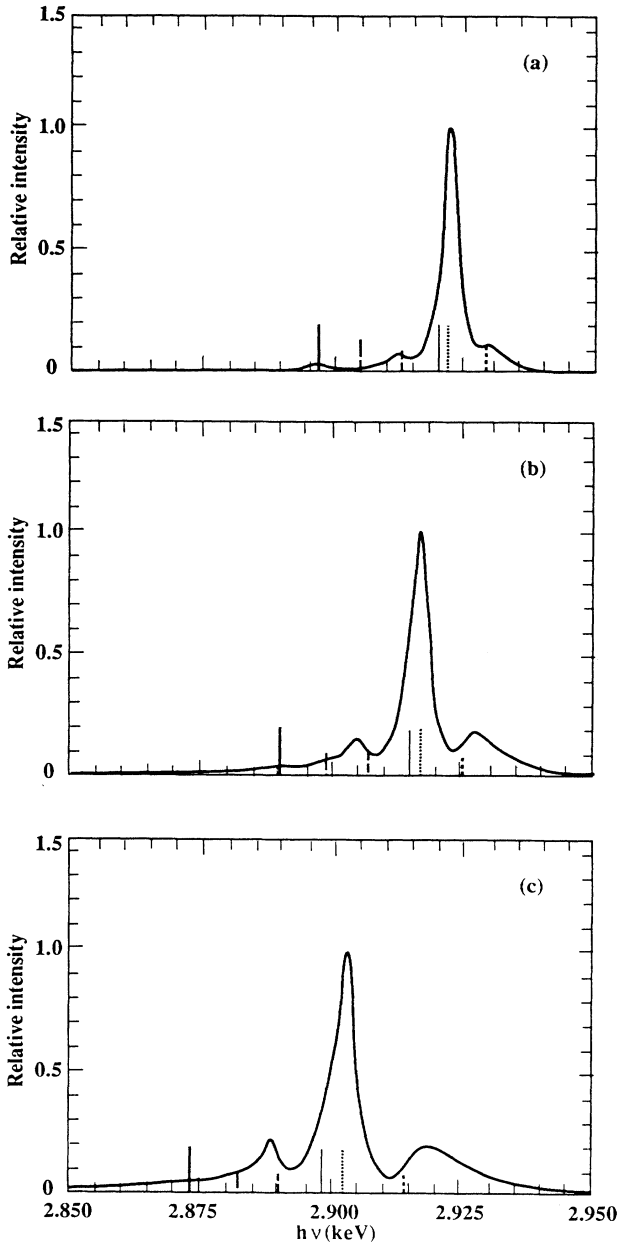

FIG. 10. The same as Fig. 8 for the $n=4\rightarrow 2p_{3/2}$ transition.

Figure 8 shows the computed spectrum obtained for the transition from $n=4$ to the $2s_{1/2}$ level. The level mixing at high density gives rise to satellites, originating from forbidden lines, which start to show up around the far wings of the lines. These satellites are still rather low for $n_i=6\times10^{21}$ cm^{-3} [see Fig. 8(a)] but grow and blur the simple line structure of the spectrum at density of $n_i=3\times10^{22}$ cm^{-3} [Fig. 8(b)], and finally at a density $n_i=1\times10^{23}$ cm^{-3} they become an emission band [Fig. 8(c)]. Similar results were obtained for the $n=4\rightarrow 2p_{1/2}$ (Fig. 9) and the $n=4\rightarrow 2p_{3/2}$ (Fig. 10) transitions.

D. The forbidden transitions

The forbidden emission band in the high-energy wing of the spectrum (Fig. 8) originates from the forbidden transitions $4d_{3/2}\rightarrow 2s_{1/2}$ and $4d_{5/2}\rightarrow 2s_{1/2}$. The intensity of this forbidden band, relative to the allowed $4p_{1/2}\rightarrow 2s_{1/2}$ transition, is a monotonically increasing function of the density, as can be seen in Fig. 11. This ratio is a fairly sensitive function of the density and may, perhaps, be used for diagnostics of hot and dense plasmas.

E. The linewidths

The spectral lines are broadened by the plasma. The linewidths as obtained from our calculations are smaller by about a factor of 2 than the widths in the spectra of Woltz and Hooper [10]. The reason for this disagreement is as yet not clear, and a more thorough investigation is required to reveal its origin. However, as the two models are so different in their basic assumptions, such a disagreement is not a surprise.

Comparison of the computed spectra with experimental results would be highly desirable. Such a comparison, if carried out with time and space integrated spectra from laser-produced plasmas, however, requires extreme caution. In fact, the temperature and density differences between the two limits of the region where Li-like krypton

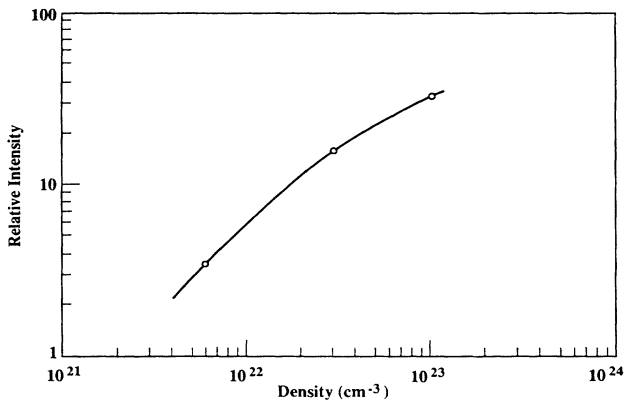

FIG. 11. Ratio of the intensity of the forbidden band to the intensity of the $4p_{3/2}\rightarrow 2s_{1/2}$ transition, as function of the ion density. The connecting line is intended as an aid to the eye.

has its highest abundance may cause significant difference in the energy shifts between photons emitted in these two limits. In a time and space integrated spectrum these shifts show up as an additional broadening mechanism. Rough estimates, based on the Thomas-Fermi model and the results of the present paper, indicate that this broadening is about 6 eV, which is approximately the same as the linewidths in the spectra shown in Ref. 9. At first sight it seems, therefore, that in a laser-produced plasma this effect can be the dominant broadening mechanism, in time and space integrated spectra, concealing the other electron and ion broadening effects. However, to give a more decisive conclusion on this issue, a simulation should be carried out with the computation of the line shift and broadening incorporated into the hydrodynamics code of the laser plasma.

ACKNOWLEDGMENTS

Part of this work was carried out when one of us (D.S.) was a visitor at the Institute of Theoretical Physics (ITP) in the University of California, Santa Barbara. He would like to express his thanks to the director Professor J. S. Langer and the staff of ITP for providing the opportunity to work in a stimulating environment and for their generous hospitality. This research was supported in part by the U. S. National Science Foundation under Grant No. PHY82-17853, supplemented by funds from the National Aeronautics and Space Administration. Support in part by National Science Foundation Grant No. PHY90-05763 is also acknowledged.

*Present address: Northeast Parallel Architechtures Center, University of Syracuse, 111 College Place, Syracuse, NY 13244.

[1] H. Griem, *Plasma Spectroscopy* (McGraw-Hill, New York, 1964).
[2] J. Stewart and K. Pyatt, Astrophys. J. **144**, 1203 (1966).
[3] B. F. Rozsnyai, Phys. Rev. A **5**, 1137 (1972).
[4] R. M. More, in *Atomic and Molecular Physics of Controlled Thermonuclear Fusion,* edited by C. J. Joachin and D. E. Post (Plenum, New York, 1983).
[5] M. W. C. Dharma-wardana and F. Perrot, Phys. Rev. A **26**, 2096 (1982).
[6] S. M. Younger, A. K. Harrison, K. Fujima, and D. Griswold, Phys. Rev. Lett. **61**, 962 (1988).
[7] S. M. Younger, A. K. Harrison, and G. Sukiyama, Phys. Rev. A **40**, 5256 (1989).
[8] J. Stein, I. B. Goldberg, D. Shalitin, and D. Salzmann, Phys. Rev. A **39**, 2078 (1989).
[9] L. A. Woltz and C. F. Hooper, Phys. Rev. A **38**, 4766 (1988).
[10] H. Griem, *Spectral Line Broadening by Plasmas* (Academic, New York, 1974).
[11] P. Malnoult, B. d'Etat, and H. Nguyen, Phys. Rev. A **40**, 1983 (1989).
[12] J. Stein, D. Shalitin, and Y. Rosenfeld, Phys. Rev. A **37**, 4854 (1988).
[13] D. Salzmann and H. Szichman, Phys. Rev. A **35**, 807 (1987).
[14] I. P. Grant, J. Phys. B **7**, 1458 (1974).
[15] G. Jamelot, P. Jaegle, P. Lemaire, and A. Carillou, J. Quant. Spectrosc. Radiat. Transfer **44**, 71 (1990).
[16] S. Goldsmith, J. Quant. Spectrosc. Radiat. Transfer **44**, 153 (1990).
[17] H. Griem, Phys. Rev. A **27**, 2566 (1983).
[18] D. K. Bradley, J. Kilkenny, S. J. Rose, and J. D. Hares, Phys. Rev. Lett. **59**, 2995 (1987).